

https://dspace.org/

Mass transfer through a porous tube

Bale, Barbara Ann

2014-10-16
http://hdl.handle.net/10539/15753

Downloaded from a DSpace repository. https://dspace.org/

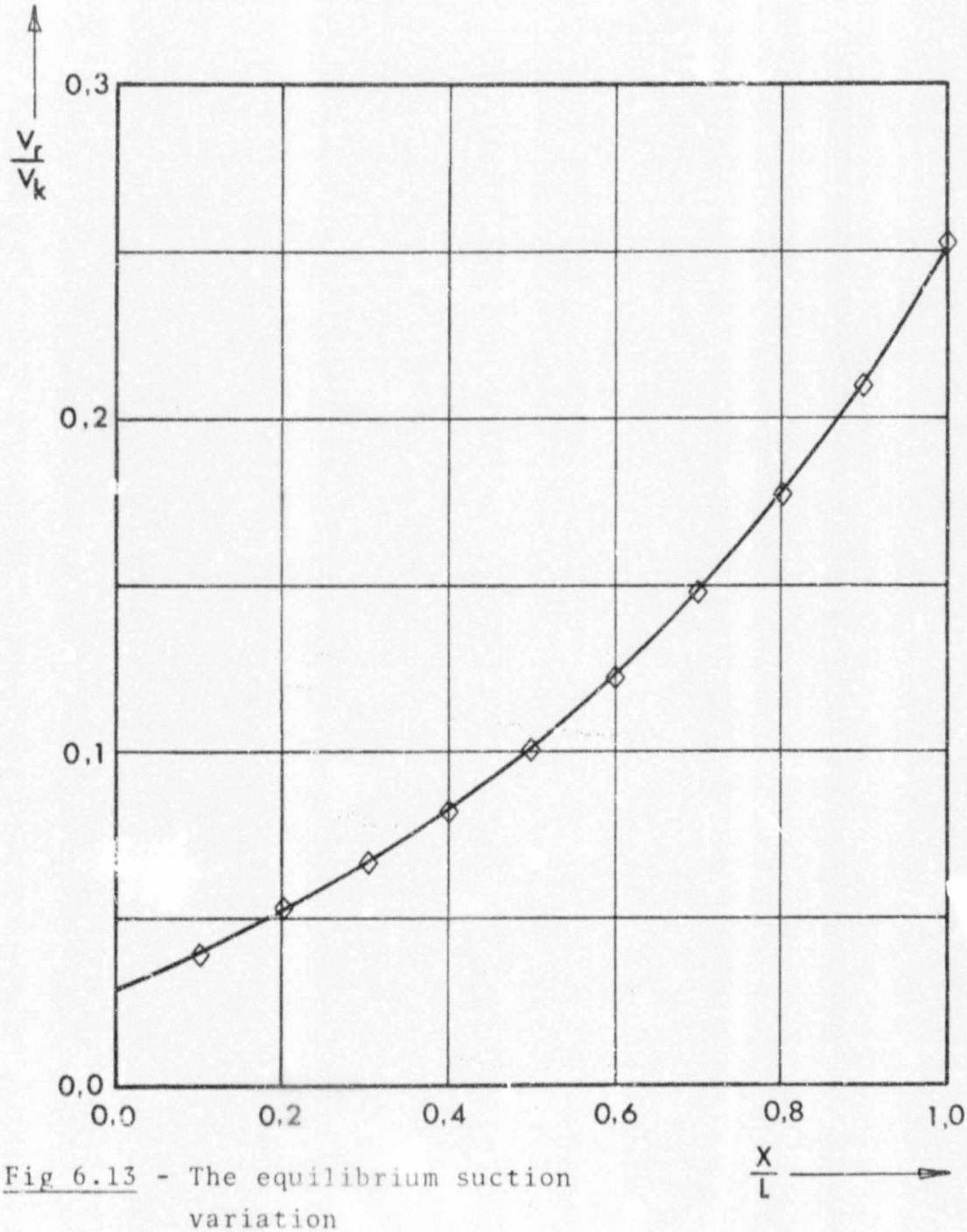


Fig 6.13 - The equilibrium suction variation

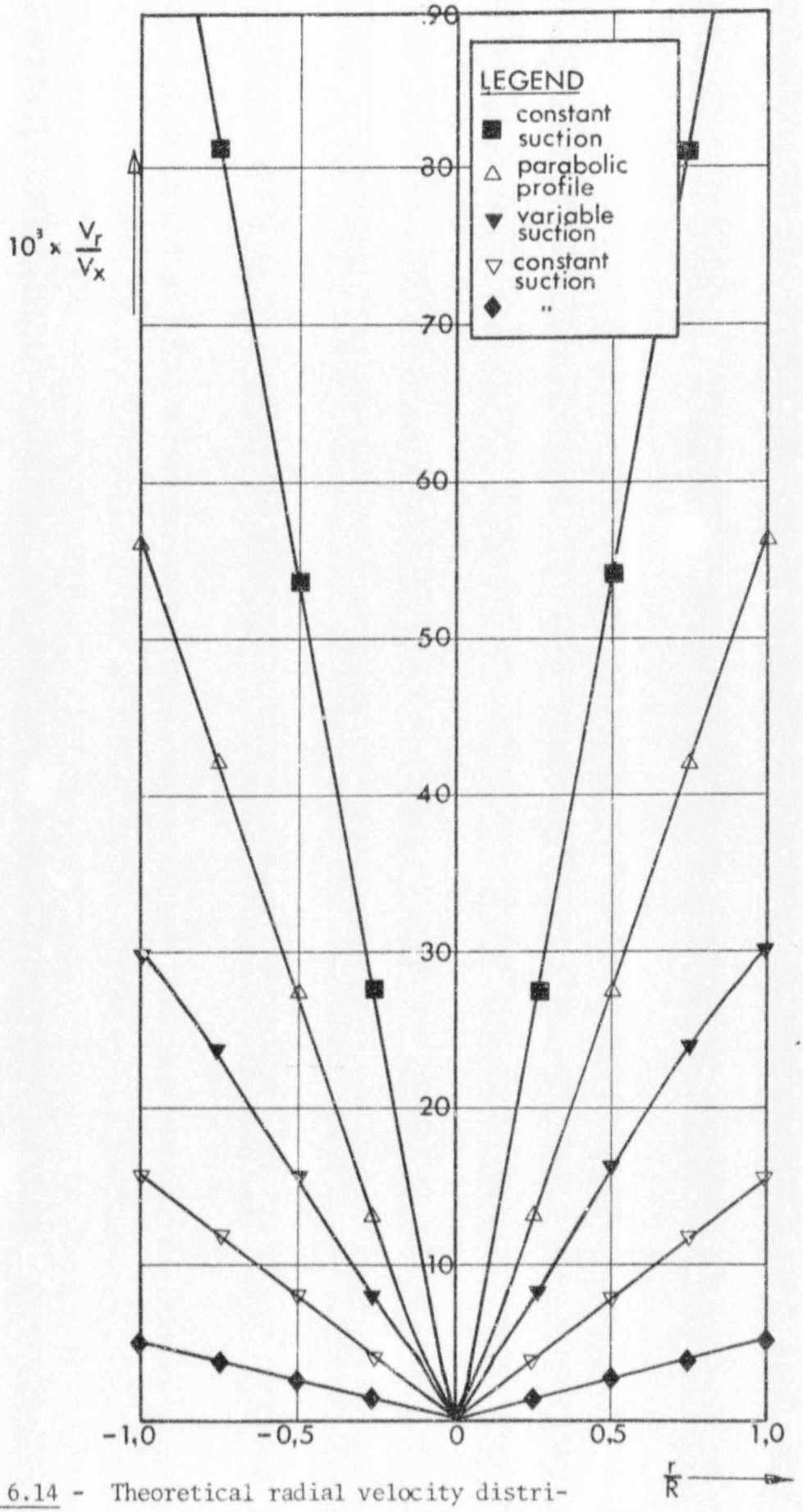


Fig 6.14 - Theoretical radial velocity distributions for various inlet velocity profiles

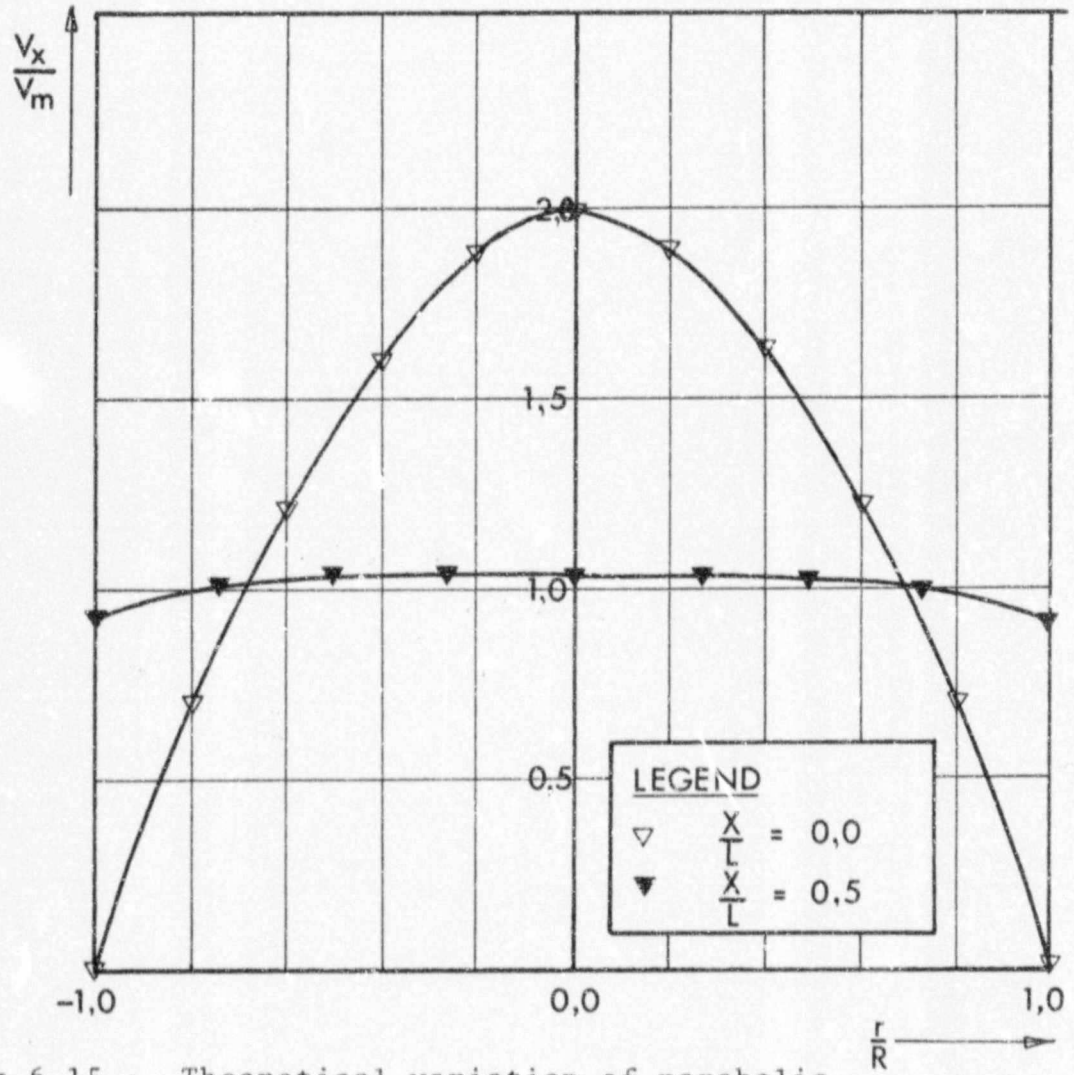


Fig 6.15 - Theoretical variation of parabolic velocity profile with suction

Figure 6.15 illustrates how an initially parabolic profile is flattened as it passes through the pipe. This is due partly to the suction and partly to the potential flow solution. The suction at the wall removes the slower moving fluid next to the wall and produces the flatter profile as shown. The flattening is also due to the fact that the potential flow model is unable to sustain the parabolic profile as the no-slip condition at the wall cannot be satisfied and gradually the parabolic profile will disappear. For the no-slip condition to be simulated it is necessary, by some means, to enter the tangential velocity at the pipe wall as a boundary condition. A method of attempting this is described in Chapter 8, during the discussion of future work.

This section has presented the theoretical results obtained from the potential flow programme. Limitations of the method that were obvious from inspecting these results have been mentioned, however, it is not possible to critically appreciate them until a comparison is made with other work in section 6.4.

6.3 The Experimental Results

The experimental data and derived quantities are tabulated in the appendix. Each table is followed by a graph showing the measured axial velocity profiles.

The experimental measurements were reduced and analysed using various formulae and techniques, these will now be discussed.

The two orifice plate results were used to calculate the volume flow rates in standard cubic meters per hour. One standard cubic meter is that quantity of air which occupies

one cubic meter when at a pressure of 1 atmosphere and a temperature of 15,5 ^{0}C. According to British Standard Code B S 1042 the working formula for the calculation of the flow rate is for dry air:

$$Q = 7{,}099 \times 10^{-3} \times C_d \times d \times E \times \sqrt{h} \times \sqrt{\frac{p}{T}} \quad . \quad . \quad . \quad (6.3.1)$$

where E is $(1 - d^2/D^2)^{-\frac{1}{2}}$
and D is the inside diameter of the piping in mm.

The constant in expression (6.3.1) allows for the inclusion of readings in the units in which the measurements were made.

Table 6.1 gives the values of the constants for both orifices.

Property	Orifice Plate 1	Orifice Plate 2
C_d	0,59	0,583
d^2 mm^2	6400	1706
d^2/D^2	0,62	0,66
E	1,62	1,71

Table 6.1 - Orifice Plate Constants

The difference between the flow rates measured by the two orifice plates gave a measure of how much air was passing through the walls of the porous pipe. The flow rates were calculated in terms of standard cubic meters so that direct comparisons could be made between runs carried out at different total pressures and temperatures. In this form the flow rates were directly proportional to the

mass flow rates. In the Appendix an anlysis of the possible errors introduced due to measurement is given and the maximum error due to measurement in a typical value of flow rate was found to be 1,8%.

The pitot tube traverse readings were taken in millimeters of water, this measured the dynamic pressure of the flow at the various radial locations. The axial velocity was calculated using expression (6.3.2)

$$V_x = \sqrt{\frac{19,6\ h_w}{\rho_{air}}}\ m/s \quad . \quad . \quad . \quad . \quad . \quad . \quad (6.3.2)$$

The maximum error in V_x due to measurements, as calculated in the appendix, is approximately 2%.

The volume flow rate calculated from the pitot-static tube readings was calculated by the integration technique described in the appendix. The result was obtained in cubic meters per hour at the working pressures and temperatures.

The mean velocity at the inlet to the porous section was calculated from expression (6.3.3):

$$V_{x_{mean}} = \frac{\text{Volume flow rate in } m^3/hr}{\text{Internal cross-sectional area in } m^2 \times 3600}\ m/s$$

$$= \frac{\text{Volume flow rate in } m^3/hr}{11,22}\ m/s \quad . \quad . \quad . \quad (6.3.3)$$

A Reynolds number, based on diameter, was calculated using the mean axial velocity evaluated from expression (6.3.3).

The pressures measured at positions 2, 3, 4, 5, 6 and 7 by means of static pressure tappings were tabulated in millimeters of mercury. The coefficient of pressure

as defined in section 3.7 was calculated using as the denominator the dynamic pressure on the axis of the pipe at static pressure tapping number 2. This position is considered close enough to the inlet of the porous pipe to indicate the dynamic pressure there (in fact it is positioned only 25,4 millimeters away). The expression for calculating the coefficient of pressure was:

$$C_{P_n} = \frac{(P_n - P_2)}{\frac{1}{2}\rho V_k^2} \times 13{,}6 \quad . \quad . \quad . \quad . \quad . \quad . \quad (6.3.4)$$

The largest error, due to inaccuracies in measurement of the pressures, in the coefficient of pressure is 6%. (See Appendix)

The hot-wire anemometer readings were obtained in volts from a digital voltmeter. These readings had to be corrected to allow for the temperature of the air. The correction formula is given in the appendix. Once this had been done it was next necessary to extract the axial and radial components of the velocity from the readings. At each location inside the pipe measurements were made with the hot-wire probe:

i) perpendicular to the axial flow
ii) parallel to the axial flow.

The voltage reading on the probes is related to the effective cooling velocity on them by the following expressions (see Appendix for more details).

$$E^2 = E_o^2 + B.U_{eff}^{0,6} \quad . \quad . \quad . \quad . \quad . \quad . \quad . \quad (6.3.5)$$

and

$$U_{eff}^2 = U_\perp^2 + kU_\parallel^2 \quad . \quad . \quad . \quad . \quad . \quad . \quad . \quad (6.3.6)$$

When the axial flow is perpendicular to the hot-wire the effective cooling velocity is given by:

$$U_{eff\perp}^2 = V_x^2 + kV_r^2 \quad . \quad . \quad . \quad . \quad . \quad . \quad (6.3.7)$$

A typical value of k is 0,04 (others are given in the Appendix) also $V_r \ll V_x$. Thus for this orientation expression (6.3.7) becomes:

$$U_{eff\perp}^2 = V_x^2 \quad . \quad . \quad . \quad . \quad . \quad . \quad . \quad (6.3.8)$$

If $E_\perp$ is the voltage output (corrected for temperature) with the hot-wire perpendicular to the axial velocity, then the axial velocity, V_x, may be read directly from the calibration curve for the probe concerned in meters per second. Inaccuracies due to reading the graphs must be included with the inaccuracies of the measuring techniques and due to this the maximum error in an axial velocity due to a hot-wire measurement is expected to be 2,5% (see Appendix).

When the axial flow is parallel to the hot-wire the effective cooling velocity is given by:

$$U_{eff\parallel}^2 = V_r^2 + kV_x^2 \quad . \quad . \quad . \quad . \quad . \quad . \quad (6.3.9)$$

Now V_r^2 and kV_x^2 may be of similar magnitudes. $U_{eff\parallel}^2$ is the effective cooling velocity read from the calibration curves for $E_\parallel$, the voltage output (corrected for air temperature) with the probe parallel to the axial velocity. V_x has been evaluated from expression (6.3.8) and so k may be obtained from figure C.8 given in the Appendix. V_r may now be calculated from expression (6.3.9).

The hot-wire anemometer readings, their corrections due to temperature and the calculations leading to the axial and radial components of the velocity are given in the Appendix.

Figure 6.16 shows curves of the pressure recovery along the porous pipe, as calculated using expression (6.3.4), for various suction rates. An average suction coefficient β_{av} is defined as:

$$\beta_{av} = \frac{\text{Volume flow rate through the porous wall}}{\text{Inside surface area of the pipe} \times V_k} \quad . \quad . \quad (6.3.10)$$

For total suction the ideal pressure recovery is $C_p = 1,0$. The two curves $\beta_{av} = 55,3 \times 10^{-3}$ and $\beta_{av} = 49,9 \times 10^{-3}$ are both for total extraction of fluid. The differences in the values of β_{av} can be seen to be well within the experimental accuracy. It can be seen that there is not quite complete pressure recovery. Although it is very close there is a percentage loss of approximately 4%. The loss is due to the skin-friction effects at the pipe wall. The other curves for different values of β_{av} take on a similar shape. As the suction decreases so the pressure recovery diminishes. There is slight scatter about the smooth curves although this is not significantly large. It is not known how the static pressure readings are affected by the porous wall. It is thought that the radial velocities are so small that the tappings will actually measure the static pressure and will not be augmented substantially due to the stagnation of the radial velocity.

Skin friction effects are not expected to be the same for the different suction rates as skin friction depends on the gradient of the velocity profile at the wall. Suction at the wall will change the velocity profile and thus the

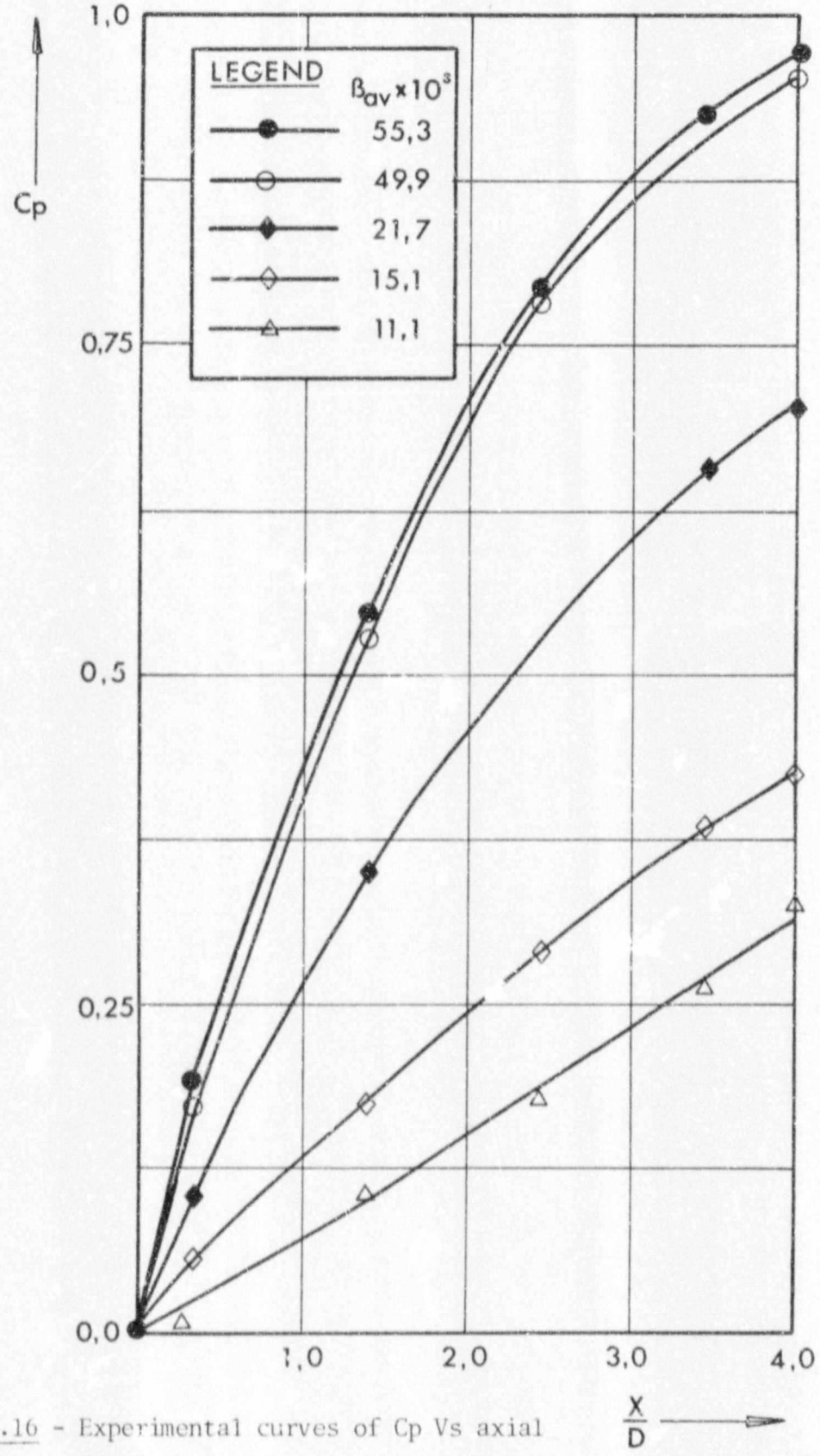


Fig 6.16 - Experimental curves of Cp Vs axial distance for various rates of mass extraction

skin friction will vary. If the curves are non-dimensionalised according to the method developed in section 6.2 then any differences between the resulting curves should be due to skin friction. The non-dimensionalised curves are illustrated in figure 6.17. Three of the curves lie on or close to one smooth curve. One curve lies above this and one below it. In the Appendix it was shown that calculated values of the pressure coefficients could be in error by up to 6% due to measurement, and so it is not possible to comment on any trend since the differences between the curves are less than 6%. It is expected, however, that the curve for $\beta_{av} = 21,7 \times 10^{-3}$ is an overestimate for the pressure recovery as it predicts no losses due to skin friction. This can be seen by comparing it with the non-dimensionalised theoretical curve, this will be done in the next section.

Figure 6.18 shows a typical set of velocity profiles measured along the porous pipe, others are given in the Appendix. At r = -31,5 mm the hot-wire probes are introduced through the pipe wall. It can be seen that the velocity readings near the wall are affected by the probe holes. There is leakage through the holes as shown by an increase in velocity in the vicinity. As the centre of the pipe is approached, however, the effects diminish and the profiles become symmetrical as shown by zero axial velocity gradient on the centre line. It is not thought that the left hand side influences the right hand side because the profile is not radially distorted, but the effects of the holes diminish long before the centre line. Only the right hand side of the graphs will therefore be examined.

The shapes of the axial velocity profile are examined by plotting each velocity relative to the mean velocity at

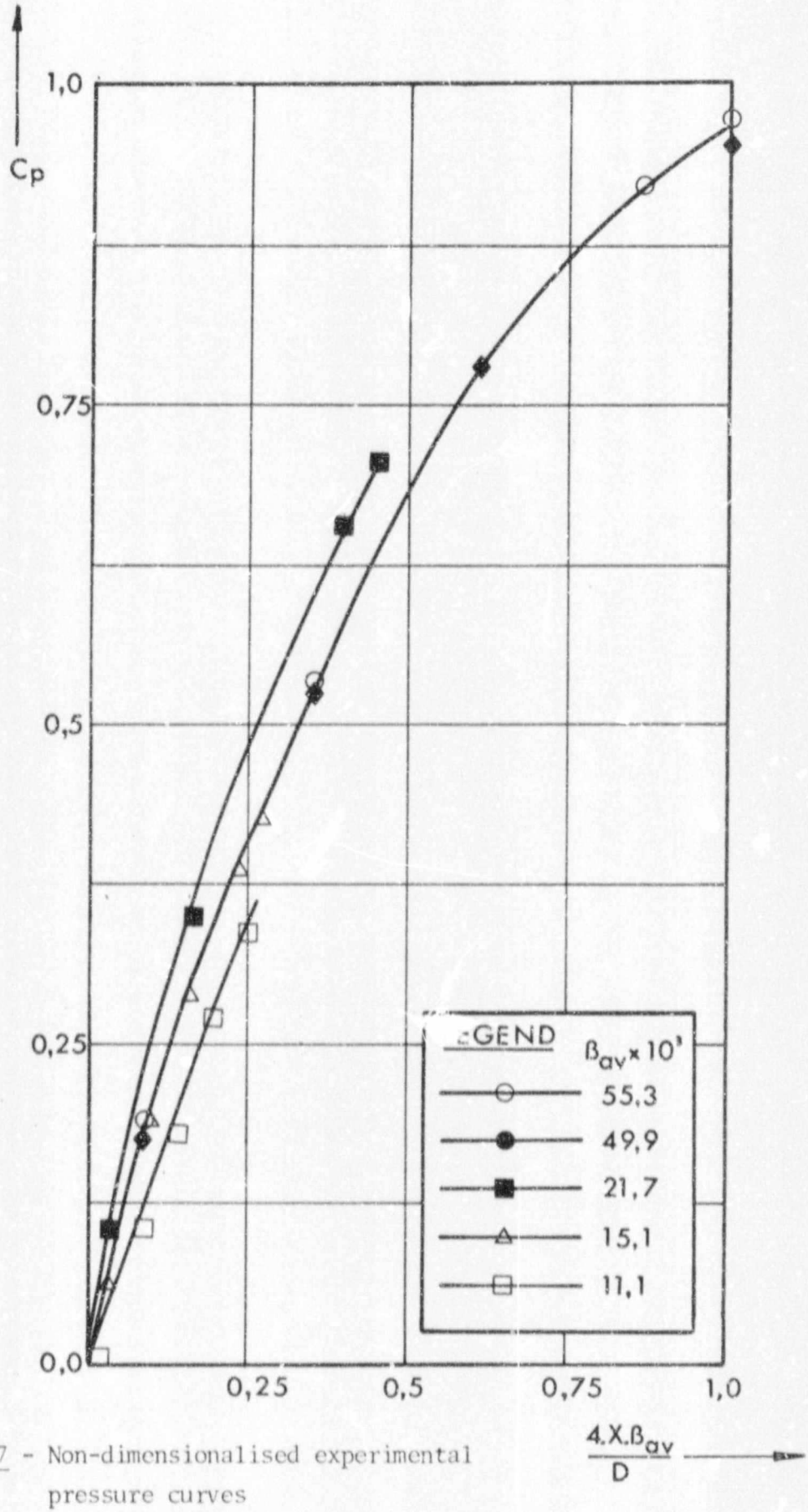


Fig 16.17 - Non-dimensionalised experimental pressure curves

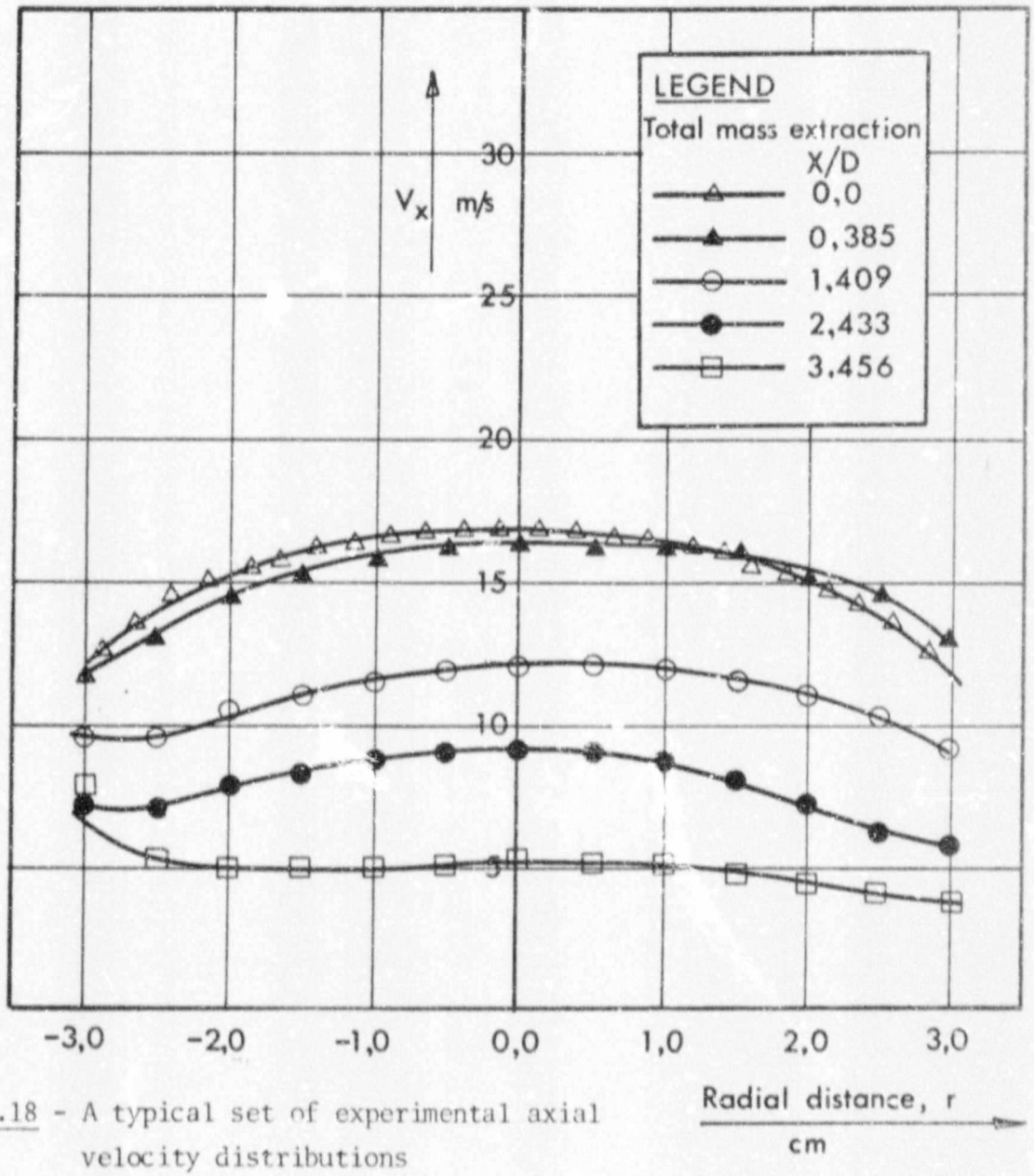


Fig 6.18 - A typical set of experimental axial velocity distributions

the same axial location. The curves obtained for several tests are shown in figures 6.19 to 6.22. In all the figures it can be noticed that the inlet profile is the flattest of all and as the suction is applied, so the tendency is for the velocity profiles to become more peaked and move towards a laminar type profile. There does not seem to be any pattern once the initial profile has changed. The profiles do not gradually become more peaked as the end of the pipe is approached. One characteristic is extremely interesting to note. The most peaked profile has a marked change in curvature as the pipe wall is approached, in some cases it actually experiences a point of inflexion. The next profile downstream after this becomes less peaked again and the curvature returns to normal. If the pipe was longer perhaps the profiles would gradually become more peaked again and also experience another inflexion point. It is difficult from such limited data to draw any definite conclusions on this phenomenum. An inflexion in a velocity profile is usually associated with a change from laminar to turbulent flow, or flow separation. Flow separation seems a little difficult to visualise in this situation as fluid is being extracted through the wall and hence is being attracted to the wall even in the presence of an adverse pressure gradient. The laminar-turbulent type transition seems more feasible. It could be that, initially the profile enters fully turbulent, but as fluid is extracted there may be relaminarization as indicated by the more peaked profiles. As the profile proceeds down the pipe fluid is sucked away, the inflexion is experienced and the boundary layer becomes unstable and reverts to a turbulent one as indicated by the flatter profiles.

It is not possible to draw the velocity profiles passing through the origin at the wall of the pipe, as it is not certain whether the no-slip condition will apply for

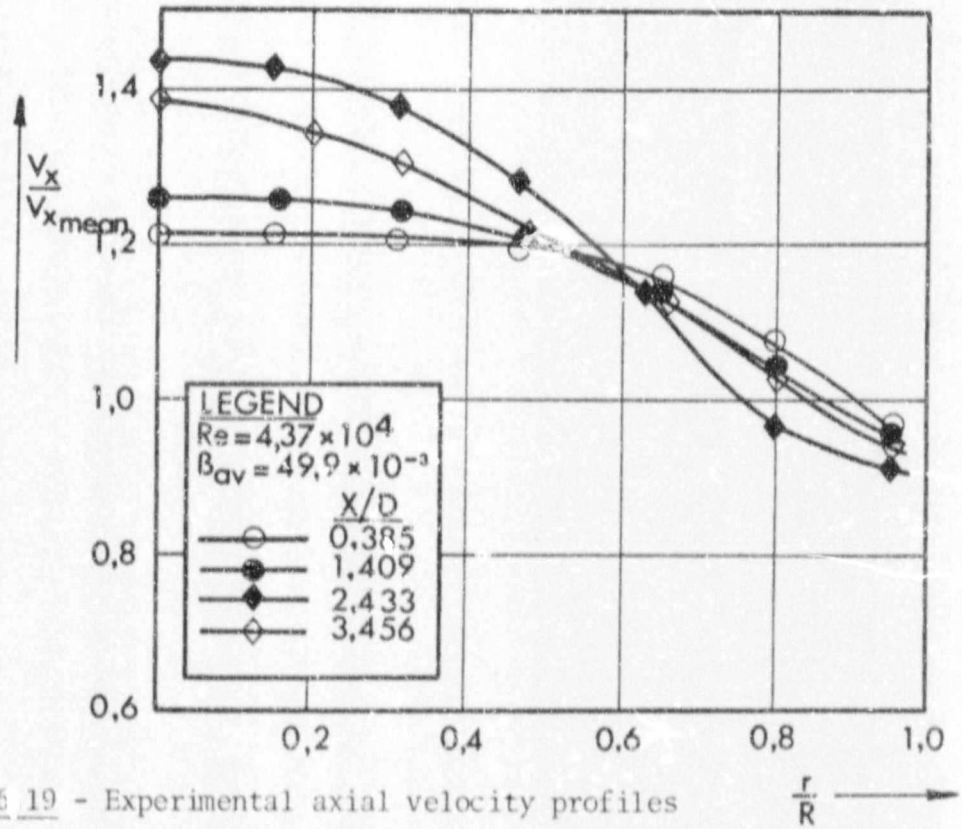


Fig 6.19 - Experimental axial velocity profiles

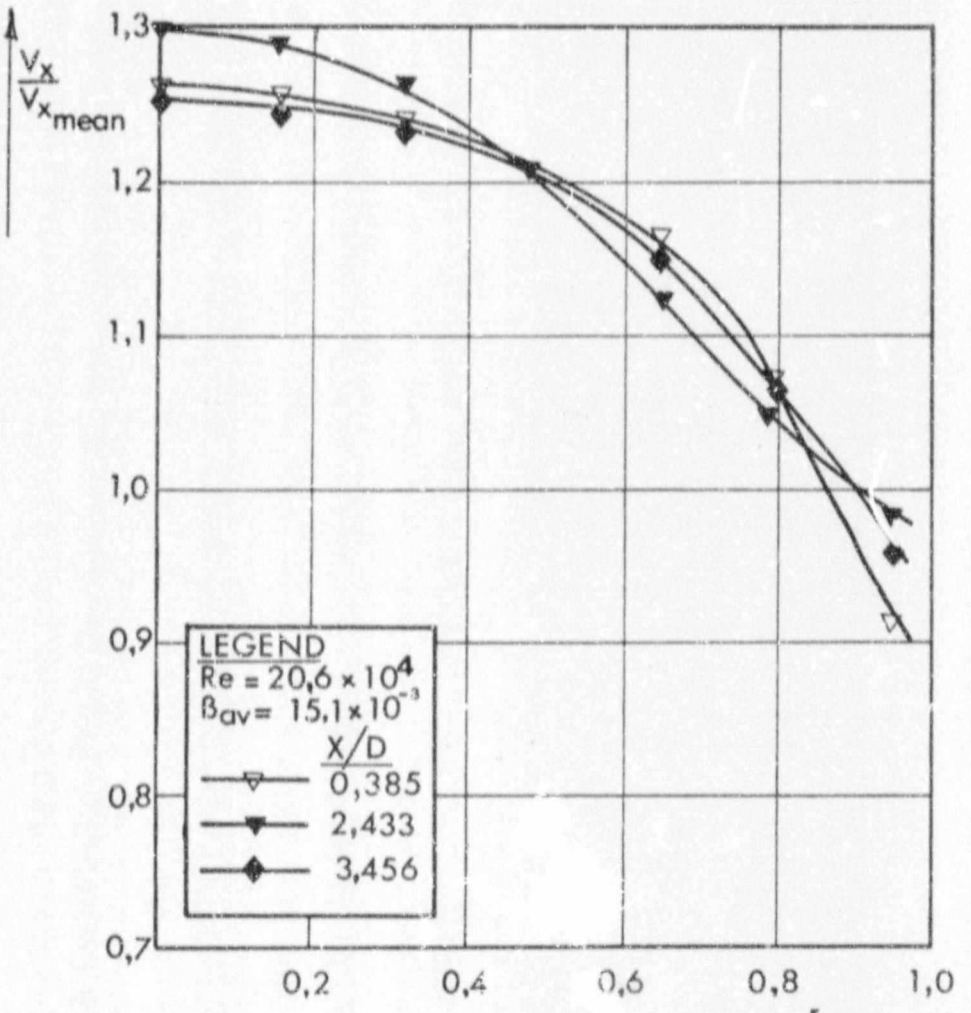


Fig 6.20 - Experimental axial velocity profiles

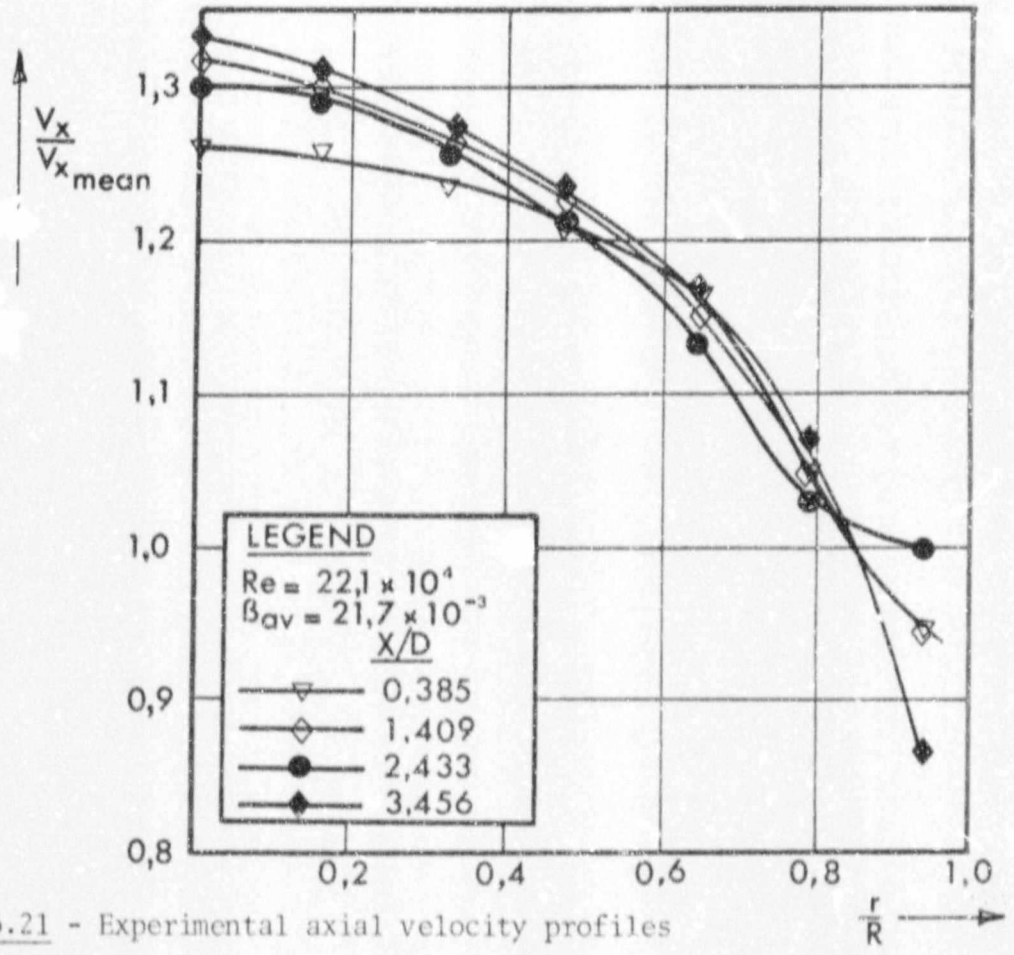


Fig 6.21 - Experimental axial velocity profiles

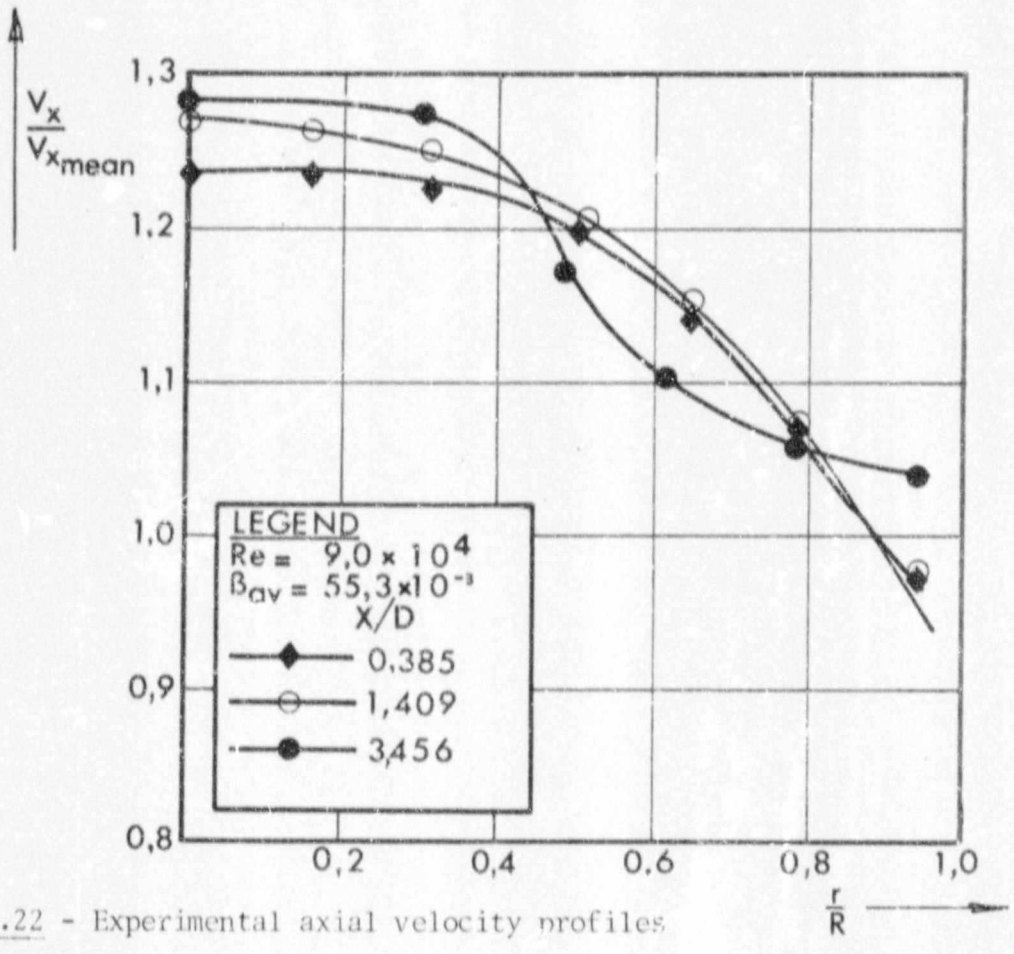


Fig 6.22 - Experimental axial velocity profiles

the porous pipe under consideration. Fluid may be able to leave the pipe through the porous walls with an axial velocity due to the structure of the bronze. Figure 6.23 illustrates this statement.

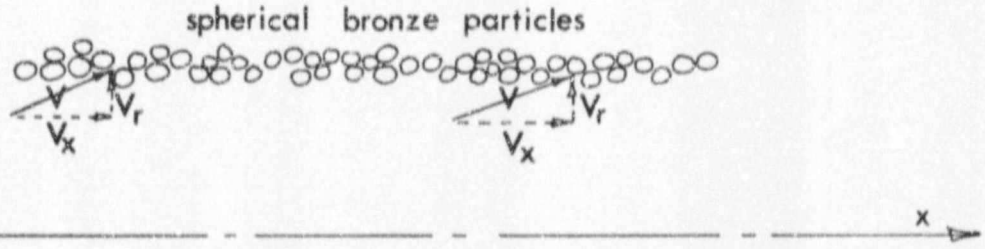


Fig 6.23 - Flow leaving the pipe with an axial velocity

This means that although the gradient of the velocity at the wall still gives a measure of the shear force on the air i e skin friction, it need not be measured at $V_x = 0,0$. Several of the profiles approach the wall with zero gradient indicating (if the no-slip condition is not satisfied) that the skin friction is zero there. Thus suction may in fact cause a decrease in skin friction.

It is indicated in the Appendix that the calculation of the radial velocities was subject to considerable inaccuracies due to the difference in magnitude between the two velocity components and inaccuracies due to transcribing results from the calibration curves. The radial velocity measurements could be in error by up to 23%. Several of the traverses have been plotted in figure 6.24. Attention should be paid to the shape of the curves rather than the magnitudes due to the uncertainty in the validity of the results. As expected the radial velocity is zero on the axis of the pipe and increases towards its maximum value at the wall of the pipe. Again only the right hand side of the profile is plotted due to the interference of the probe holes. The curves are not linear but are

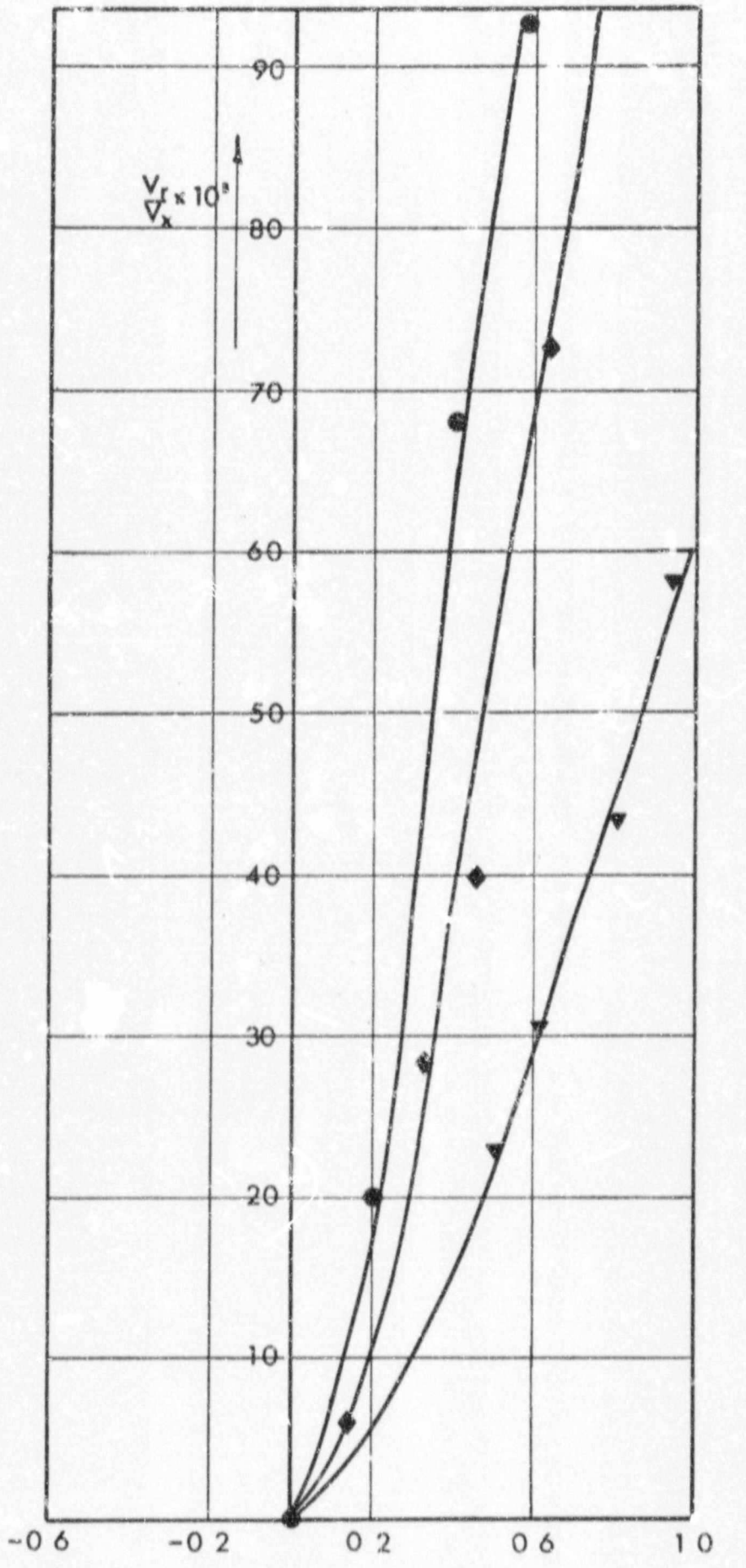


Fig 6.24 - Experimental variations of radial velocity across the pipe

slightly concave. If the tables in the Appendix are studied it can be seen that some of the radial velocity profiles are slightly irregular, and experience the occasional drop in radial velocity as the wall is approached. This is due to the sensitivity that the radial velocity calculations exhibit with slight inaccuracies due to measurement. The radial velocities at the wall appear to be overestimated as compared with the average suction velocity required for a given mass extraction. A possible explanation for this is the wall effect on the hot-wire. The wire loses heat due to the cooling effect of the air and also by radiation to the wall, thus an overestimate of the cooling velocity is made and hence an overestimate of the suction velocity.

To measure the radial velocities more accurately a different method must be devised. It may be possible to use crossed probe hot-wires, but it is thought that these may experience the same difficulties due to the difference in magnitudes between the two velocity components.

6.4 Comparison of the theoretical and experimental results and work done by other authors

There were many difficulties encountered when trying to compare results between various authors. The main ones were due to the way in which other research has been presented. Frequently, insufficient data was presented and so it became impossible to non-dimensionalise with respect to the same variables and comparisons became impossible.

Figure 6.25 shows experimental results of Aggarwal et al [25] illustrating the rise in pressure obtained along the porous pipe for various values of α, an extraction coefficient. Where α is defined by:

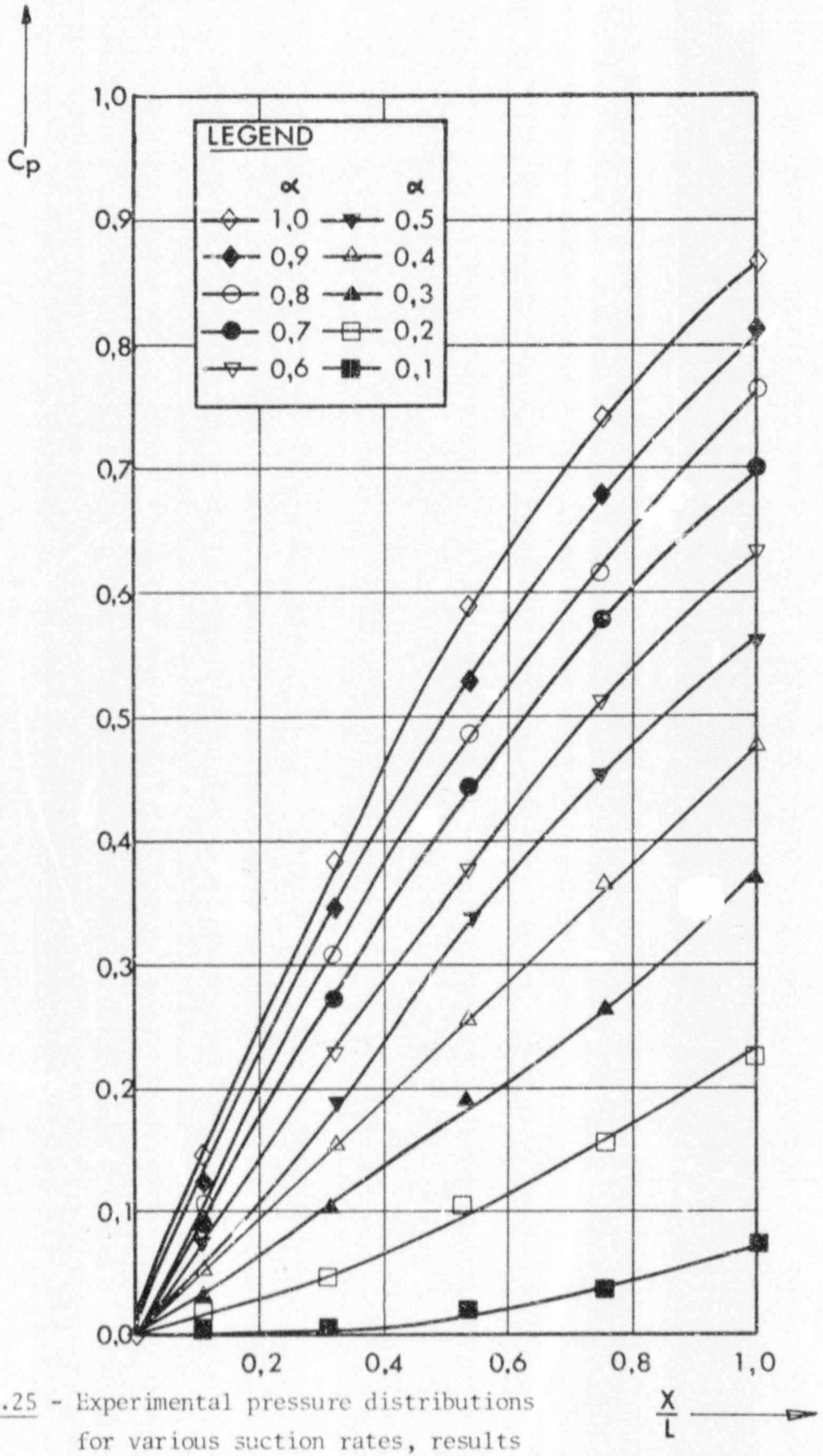


Fig 6.25 - Experimental pressure distributions for various suction rates, results of Aggarwal et al [25].

$$\alpha = \frac{\text{Mass flow rate extracted through the sides}}{\text{Mass flow rate flowing axially into the pipe}}$$

$$= \frac{2\pi RL\ V_r}{\pi R^2 V_{x\,mean}} = \frac{2\ V_r}{V_{x\,mean}}\ \frac{L}{R} \quad . \quad . \quad . \quad . \quad . \quad (6.4.1)$$

The ratio $V_r/V_{x\,mean}$ is related to β, the suction coefficient. For a turbulent velocity profile the mean velocity is 0,814 of the maximum axial velocity and for a laminar parabolic profile it is half the maximum. Thus for turbulent flow:

$$\alpha = 2,46\beta\frac{L}{R} \quad . \quad . \quad . \quad . \quad . \quad . \quad . \quad (6.4.2)$$

and for laminar flow:

$$\alpha = 4\beta\frac{L}{R} \quad . \quad . \quad . \quad . \quad . \quad . \quad . \quad . \quad (6.4.3)$$

The curves of figure 6.25 are similar in shape to the theoretical curves of the present theory which were illustrated in figure 6.2 and the experimental results shown in figure 6.16. The actual pressure recoveries due to a given suction rate, however, are lower than predicted. To compare the three sets of results it is useful to collapse the pressure curves of figure 6.25 by means of the non-dimensionalising process described in section 6.2. The resulting curves are illustrated in figure 6.26. For the high suction rates the curves collapse within experimental accuracy onto one curve, indicating that the effects of skin friction are similar for these flow situations. As the lower suction rates are approached, so the points deviate from the standard curve indicating an increase in skin friction.

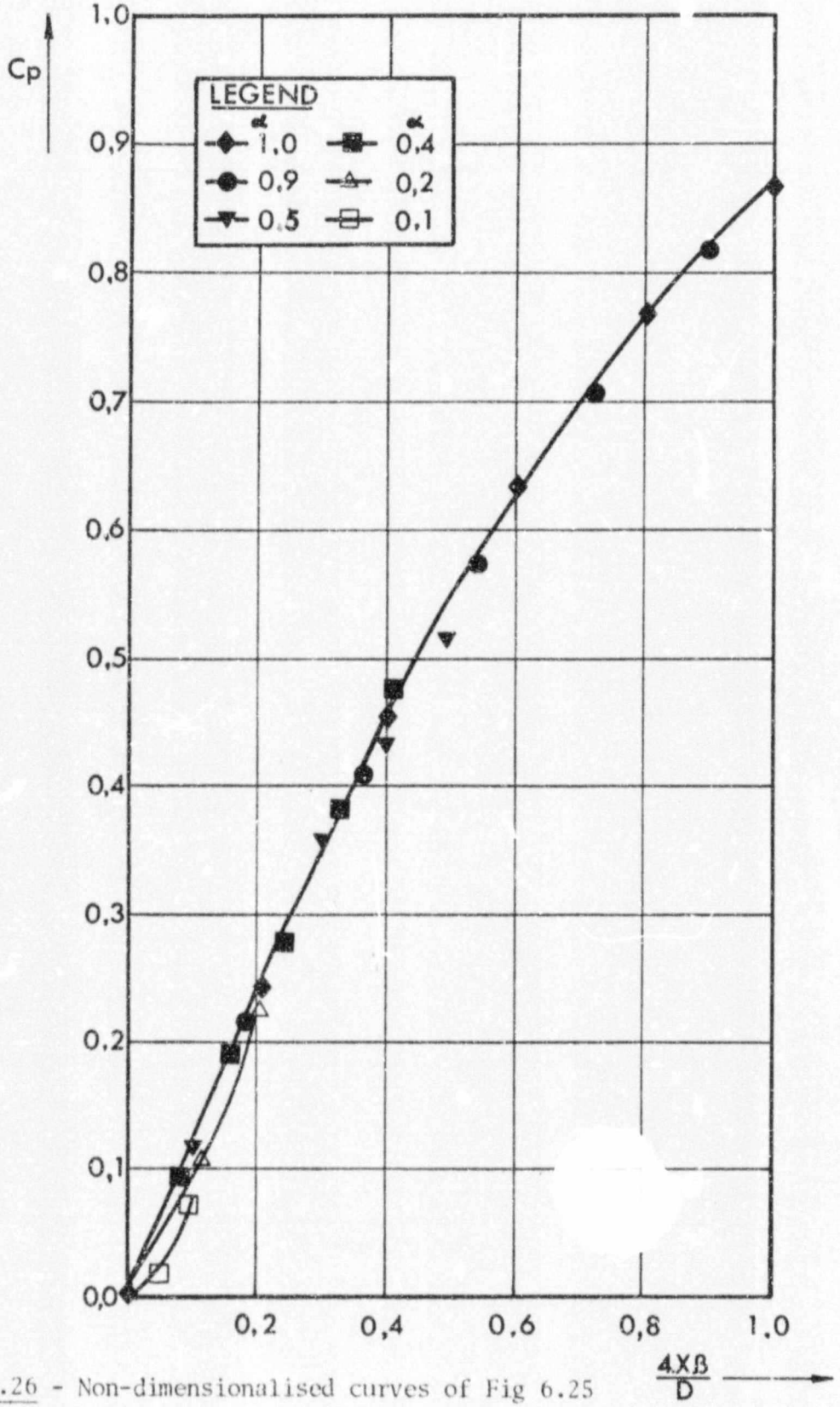


Fig 6.26 - Non-dimensionalised curves of Fig 6.25

Figure 6.27 compares the present theory and experimental results with experiments performed by Aggarwal et al [25] and Berger and Blake [18]. The results have been non-dimensionalised with respect to the suction coefficient. Differences between the experiments and the theory must be due entirely to skin friction effects, and the errors due to measurements. The three experiments exhibit varying proportions of skin friction. The present experiments agree to within 5% of the theoretical results, and appear to be effected less by friction than the other results. All three experiments were conducted with porous bronze specimens made by the same manufacturers, however, they were of different porosities. Aggarwal et al conducted their experiments with specimens of Grade A porosity (see section 5.4), Berger and Blake with Grade C and the present ones were performed with grade D. There appears to be an agreement. It seems that the smaller the porosity the greater the skin friction. This can be explained with reference to figure 6.23. The smaller porosity pipes are made from smaller spherical particles of bronze. This means that there is less likelyhood for the fluid to be able to leave through the wall with an axial velocity and the no-slip condition is probably met. As the spherical particles increase in size, and hence the porosity increases, the no-slip condition may be violated and the skin friction is reduced as indicated in figure 6.27.

The limitations of the potential flow theory are obviously the inability to predict skin friction, however, the shape of the curves are all very similar and as a starting point in an analysis the potential flow theory gives a reasonable approximation to the real flow situation. It is expected that if the no-slip condition could be simulated in the potential theory the theoretical and

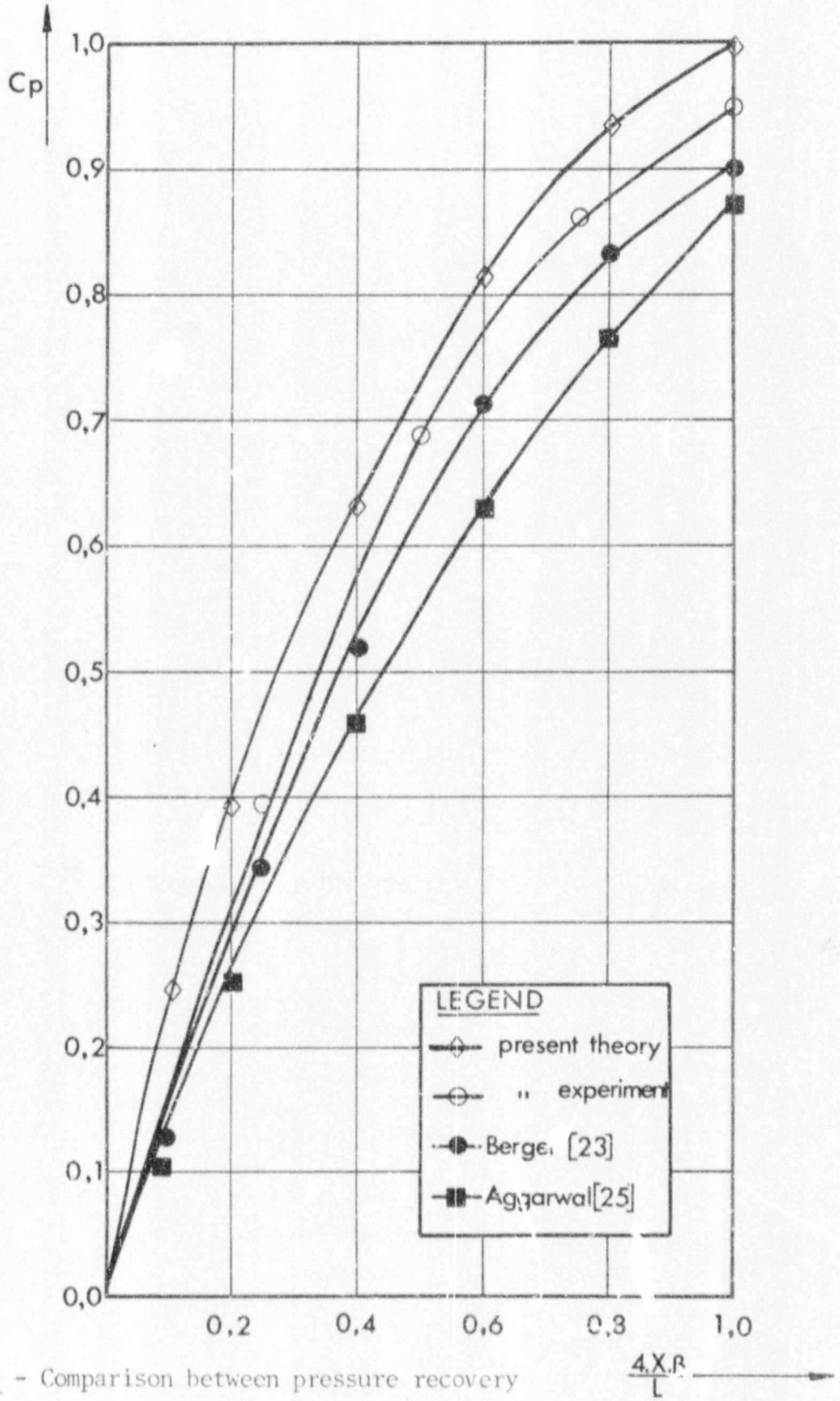


Fig 6.27 - Comparison between pressure recovery predictions from various sources

experimental curves would agree more closely. It is evident from the curves that the physical nature of the porous material plays an important part in the actual pressure recoveries achieved and any theories will have to incorporate this.

Figure 6.28 shows a comparison of the potential flow theory and a theory developed by Yuan & Finkelstein [11] for uniform blowing into the porous pipe. The two are in very close agreement. There is no data available for comparisons with experimental results.

Figure 6.29 shows experimental velocity profiles measured by Aggarwal et al [25]. The axial velocity has been non-dimensionalised with respect to the mean axial velocity. The four profiles shown are obtained at the end of the porous pipe for various suction rates. One profile has almost become a laminar one as indicated by the parabolic profile. This is for practically total suction. One of the profiles exhibits an inflexion point as was experienced by the experimental results given in section 6.3. Figure 6.30 shows theoretical predictions of velocity profiles for various suctions in laminar flow. These profiles were obtained by F M White [14] and are typical of those achieved with similarity solutions. The profiles become more peaked as the suction increases and have an inflexion for certain extraction rates. For large suction they also predict reverse flow at the wall. This has never been substansiated by experiment.

Figure 6.29 shows that, according to Aggarwal et al the net effect of suction is to make the velocity profile fuller at modest suction and to make it more peaked as the suction rate becomes greater. Weissburg [15] also found that velocity profiles became fuller at low rates

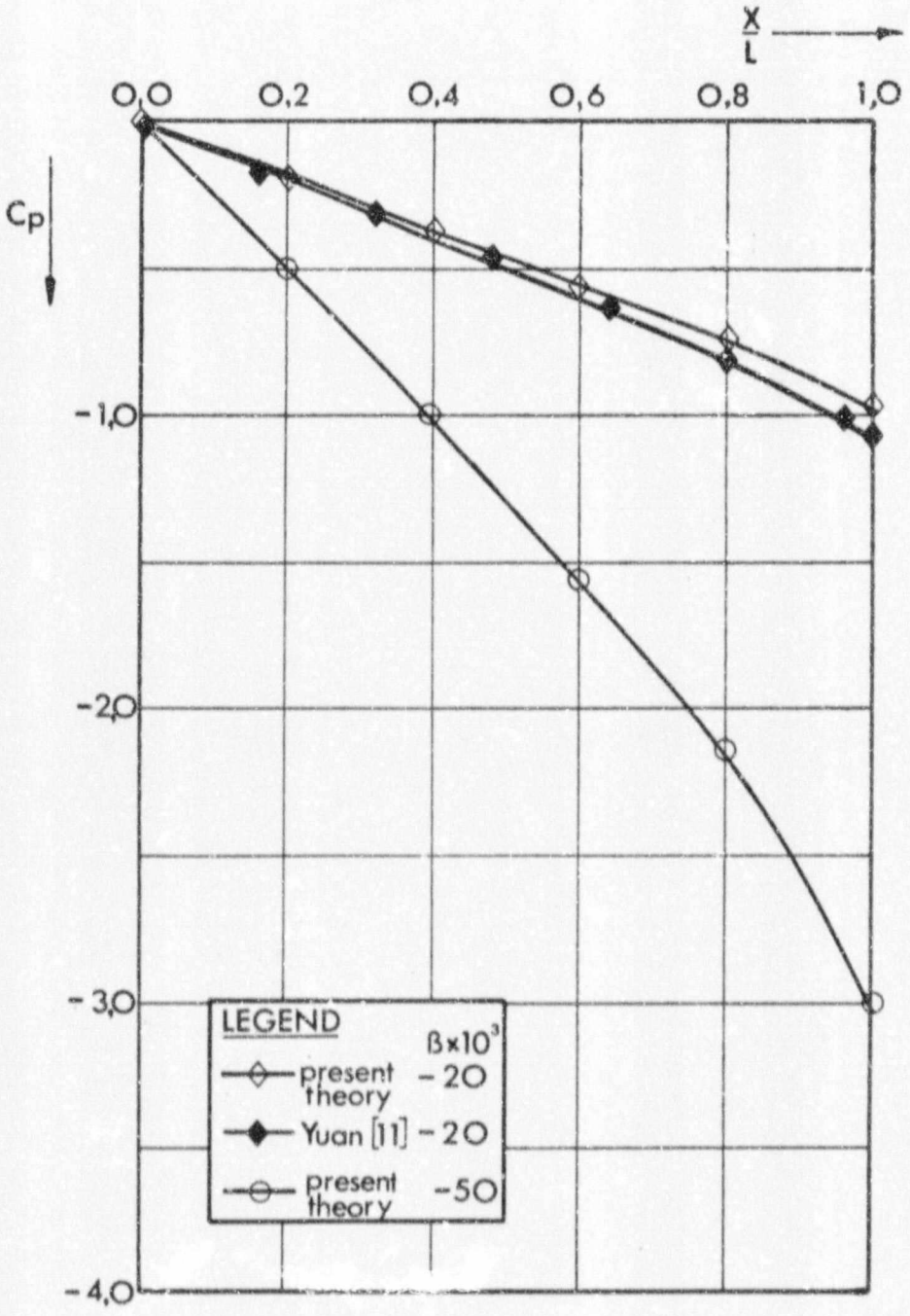


Fig 6.28 - Comparison between two theories of pressure drop with blowing

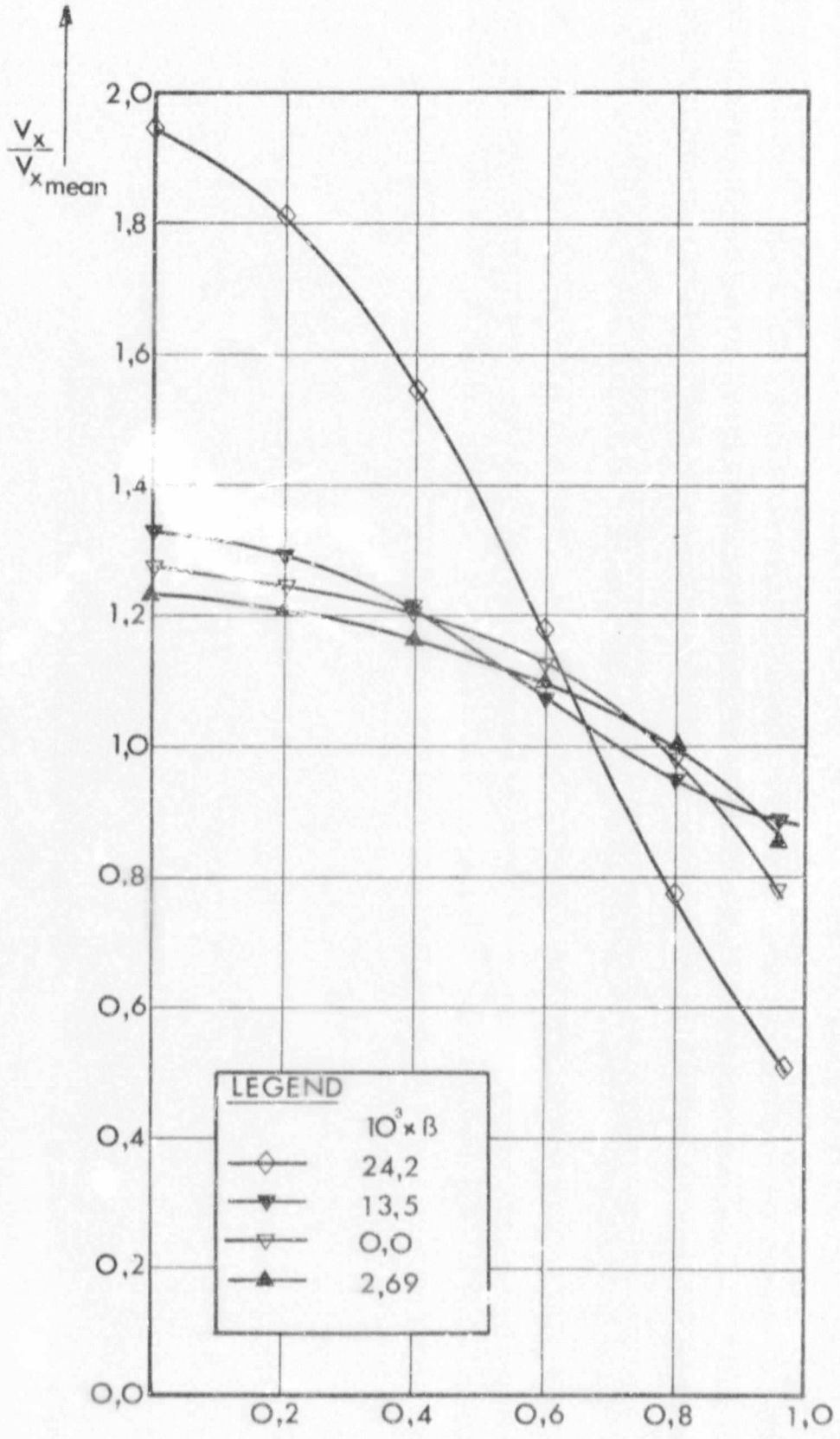


Fig 6.29 - Experimental velocity profiles obtained by Aggarwal et al [25]

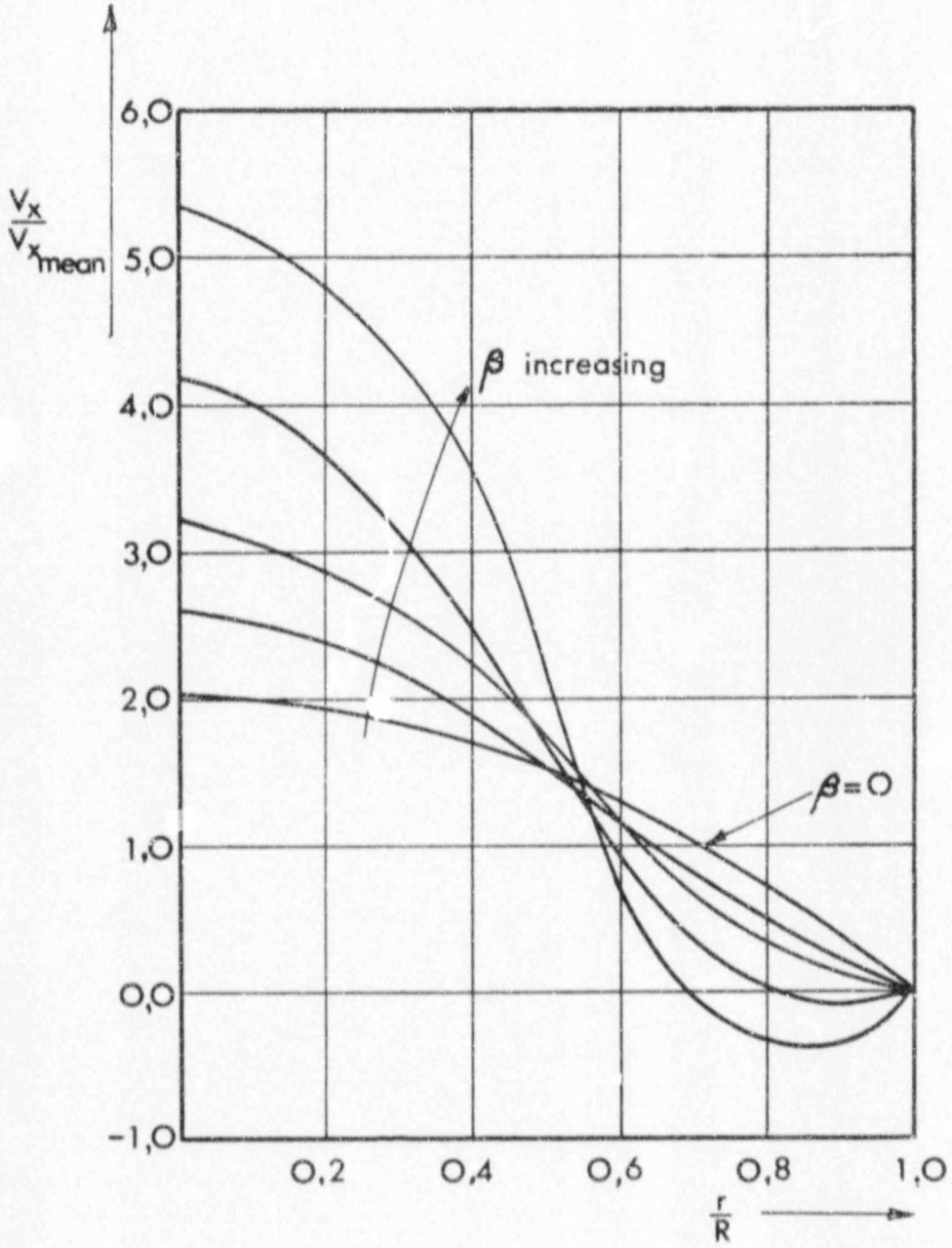


Fig 6.30 - Typical velocity profiles obtained from similarity solutions

Author Bale Barbara Anne
Name of thesis Mass Transfer Through A Porous Tube. 1975

PUBLISHER:
University of the Witwatersrand, Johannesburg
©2013

LEGAL NOTICES:

Copyright Notice: All materials on the University of the Witwatersrand, Johannesburg Library website are protected by South African copyright law and may not be distributed, transmitted, displayed, or otherwise published in any format, without the prior written permission of the copyright owner.

Disclaimer and Terms of Use: Provided that you maintain all copyright and other notices contained therein, you may download material (one machine readable copy and one print copy per page) for your personal and/or educational non-commercial use only.

The University of the Witwatersrand, Johannesburg, is not responsible for any errors or omissions and excludes any and all liability for any errors in or omissions from the information on the Library website.